41st Aerospace Sciences Meeting and Exhibit
6-9 January 2003, Reno, Nevada

AIAA 2003-1068

Aerodynamic Design of Cascades by Using an Adjoint Equation Method

Shuchi Yang,* Hsiao-Yuan Wu,† and Feng Liu‡
Department of Mechanical and Aerospace Engineering
University of California, Irvine, CA 92697-3975

Her-Mann Tsai§
Temasek Laboratories
National University of Singapore
Kent Ridge Crescent, Singapore 119260

A continuous adjoint equation method is developed for the aerodynamic design of cascade blades in a two-dimensional, inviscid, and compressible flow. A cost function based on a prescribed target pressure distribution is defined and the purpose of design is to minimize the value of the cost function. The adjoint equations and the corresponding boundary conditions are derived based on the Euler equations, the flow boundary conditions, and the definition of the cost function. Gradient information is obtained by solving the adjoint equations. A one-dimensional search algorithm is used to perform the optimization in the calculated gradient direction. Multigrid method is applied to accelerate the computation for both the Euler and the adjoint equations. Three transonic cascade blade design cases are tested. The results show that the method is effective and efficient for turbomachinery blade design. The effect of shape functions on the performance of the design method is discussed.

I. Introduction

CFD-based design methods can be broadly classified into two basic categories: inverse methods and numerical optimization methods. Inverse methods solve the inverse problem of determining the shape given a pressure distribution. A classical example of inverse design was the conformal mapping method by Lighthill[1] for two-dimensional incompressible flows. Bauer, Garabedian and Korn designed supercritical wing sections using inverse hodograph methods.[2] Hobson designed two shock free impulse cascades by hodograph method.[3] Inverse design for turbomachinery cascades were studied by Tan et al.[4] and Giles et al.[5] Dang et al.[6,7] developed an inverse method where only the pressure difference on the blade surfaces are specified instead of velocity distributions.

Inverse methods are relatively fast in computation. However, the user must be highly experienced to prescribe the appropriate surface flow distributions and initial guesses of the geometry. Even with that given, there is in general no guarantee that such an objective is attainable. And if it is, it may not be the optimal.

Aerodynamic optimization has been a topic studied since the early days of aerodynamics. It was not until recently, however, that systematic computer optimization procedures were developed to optimize the design of airfoils and wings involving nonlinear flows. This was only made possible by the new capability of calculating complex nonlinear flows within short computational time and the advances in nonlinear optimization techniques. The basic idea of these methods is to couple a fast CFD analysis code with a numerical optimization scheme. The CFD analysis code is used to evaluate an aerodynamic measure of merit, which the optimization method uses to extremize by modifying a given set of design variables. Hicks et al.[8] used numerical optimization for transonic airfoil shape design with a transonic potential code. Reuther et al.[9] used an optimization method with the Euler equations for the design of supersonic wing-body configurations. Hager et al.[10] considered transonic airfoil optimization using the Navier-Stokes equations. With these methods any reasonable aerodynamic quantity can be used as a design objective. If a surface pressure distribution is specified as a target function, the method will also mimic an inverse method to find out the particular shape that gives the desired pressure distribution. If this pressure distribution is not attainable, the optimization method will not fail as an inverse method would, but rather it will provide a best approximation to the given distribution.

*Post-doctoral Researcher.
†Graduate Researcher, AIAA Student Member.
‡Associate Professor, AIAA Member.
§Principal Research Scientist, AIAA Member.

The numerical optimization methods used by the authors cited in the above paragraph use direct perturbation and finite-differences to obtain the gradient of the cost function with respect to the design variables. This makes such methods extremely expensive for relatively large number of design variables because the large number of flow solutions needed to determine the gradient information. An alternative way is the adjoint equation method. Gradient information can be obtained by solving the adjoint equations of the flow governing equations. The computational time of solving the adjoint equations is approximately the same as that of solving the flow equations, and it is independent of the number of design parameters. Therefore, this method is far more efficient than the direct perturbation method when the number of design parameters is large.

Jameson pioneered optimization of airfoils and wings by using the adjoint equation method first for the potential equation[11] and for the Euler equations.[12] Reuther and Jameson considered wings and wing-body combinations with arbitrary curvilinear grids.[13] There have been major progresses in the last few years in the development of adjoint method for external flows.[14, 15] However, there has been little work done on turbomachinery blades. The goal of this paper is to develop and evaluate the same adjoint equation method as in Ref. 12 for cascade blade optimization. Initial application is restricted to inverse design by using the adjoint optimization method with a cost function based on specified pressure distribution. Attention is paid to the boundary conditions for cascade flow problems. The flow solver and the adjoint solver are modified from Flo52x. The code is validated by comparing the gradient calculated by the adjoint equation method with that calculated by the direct perturbation method. Then three transonic cascade design cases are tested. The target designs are a cascade using the NACA0015 airfoil, the Hobson I cascade, and the Hobson II cascade. Finally, the effect of the distribution and the number of shape functions are discussed in connection with the performance of the optimization program.

II. Inverse Design as an Optimization Problem

Inverse design problems of two-dimensional turbomachinery cascades are studied based on the Euler equations. Figure 1 is a sketch of the domain. Periodic boundary conditions are applied on the upper boundary and the lower boundary. At the inlet, the stagnation pressure, the stagnation density, and the angle of the flow are specified. At the exit, the static pressure is specified. A target pressure distribution p_d is given on the blade. The purpose is to modify the initial blade shape to obtain the target pressure distribution. The

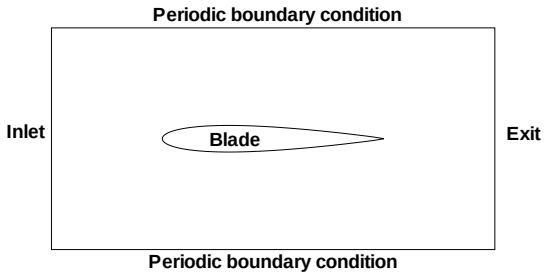

Fig. 1 Domain of a cascade blade passage.

cost function is defined as:

$$I = \frac{1}{2}\int_{B_W}(p - p_d)^2 dB_W \tag{1}$$

in which B_W is the blade surface, p is the pressure. A smaller value of the cost function means the design is closer to the target design. The chord length is fixed and normalized to be one.

III. Optimization by an Adjoint Equation Method

A. The Adjoint Equations

The continuous adjoint equations are derived based on the general approach proposed by Jameson.[12] In general, the cost function I is a function of the blade shape $\mathcal{F}$ and the flow field $\mathbf{w}$, i.e.,

$$I = I(\mathcal{F}, \mathbf{w})$$

where the flow field $\mathbf{w}$ are related to $\mathcal{F}$ by the flow governing equation

$$\mathbf{R}(\mathcal{F}, \mathbf{w}) = 0$$

subject to appropriate boundary conditions. If the shape is changed, the flow field is also changed so that the variation of the cost function is

$$\delta I = \frac{\partial I}{\partial \mathcal{F}}\delta\mathcal{F} + \frac{\partial I}{\partial \mathbf{w}}\delta\mathbf{w}$$

The $\delta\mathcal{F}$ term can be obtained directly from geometry, but the $\delta\mathbf{w}$ term will need flow field evaluations, which are time consuming. In order to eliminate the explicit dependence on $\delta\mathbf{w}$, the following procedure is applied. Taking the variations of the flow governing equations, we have

$$\delta\mathbf{R} = \frac{\partial \mathbf{R}}{\partial \mathcal{F}}\delta\mathcal{F} + \frac{\partial \mathbf{R}}{\partial \mathbf{w}}\delta\mathbf{w} = 0$$

Introducing an arbitrary multiplier $\mathbf{\Phi}$, we may write

$$\delta I = \frac{\partial I}{\partial \mathcal{F}}\delta\mathcal{F} + \frac{\partial I}{\partial \mathbf{w}}\delta\mathbf{w} - \mathbf{\Phi}^T\left(\frac{\partial \mathbf{R}}{\partial \mathcal{F}}\delta\mathcal{F} + \frac{\partial \mathbf{R}}{\partial \mathbf{w}}\delta\mathbf{w}\right)$$

or,

$$\delta I = (\frac{\partial I}{\partial \mathbf{w}} - \mathbf{\Phi}^T \frac{\partial \mathbf{R}}{\partial \mathbf{w}})\delta \mathbf{w} + (\frac{\partial I}{\partial \mathcal{F}} - \mathbf{\Phi}^T \frac{\partial \mathbf{R}}{\partial \mathcal{F}})\delta \mathcal{F}$$

To eliminate the explicit dependence on $\delta \mathbf{w}$, let

$$\frac{\partial I}{\partial \mathbf{w}} - \mathbf{\Phi}^T \frac{\partial \mathbf{R}}{\partial \mathbf{w}} = 0$$

This is the adjoint equation. The solution $\mathbf{\Phi}$ is called the co-state variable. Once $\mathbf{\Phi}$ is obtained, we have $\delta I = \mathbf{G}\delta\mathcal{F}$, where $\mathbf{G} = \frac{\partial I}{\partial \mathcal{F}} - \mathbf{\Phi}^T \frac{\partial \mathbf{R}}{\partial \mathcal{F}}$ is the needed gradient of I with respect to the shape change $\delta\mathcal{F}$. Once the gradient is known, $\delta\mathcal{F}$ can be chosen to have a negative δI to reduce the cost function. After several design cycles, when the cost function approaches zero, the target design is accomplished.

The above general procedure can be applied to the Euler equations and the cost function defined by Eqn. (1). The detailed formulation used here follows that in the works of Reuther[16] and Wang.[17] However, their works concern airfoil optimization for external flows. For internal flows such as a cascade flow, the boundary conditions need to be changed. Consider the physical domain (x_1, x_2) and the computational domain (ξ_1, ξ_2). The flow field shown in Figure 1 is mapped to a rectangular area on the (ξ_1, ξ_2) plane with an O-mesh configuration in which $\xi_2 = 0$ corresponds to the blade surface B_W. Let B_C be the outer boundary of the domain, which consists of the inlet, the exit, and the two periodic boundaries. The Euler equations in the (x_1, x_2) domain can be written as

$$\frac{\partial \mathbf{w}}{\partial t} + \frac{\partial \mathbf{f}_i}{\partial x_i} = 0 \quad (i = 1, 2) \tag{2}$$

in which t is time, $\mathbf{w}$ is the conservative variable vector, and $\mathbf{f}_i$ are the flux vectors. The flow boundary conditions are described in the previous section.

A variation of the shape will cause a variation δp of the pressure and consequently a variation in the cost function:

$$\begin{aligned} \delta I &= \int_{B_W} (p - p_d)\delta p \frac{dB_W}{d\xi_1} d\xi_1 \\ &\quad + \frac{1}{2}\int_{B_W} (p - p_d)^2 \delta(\frac{dB_W}{d\xi_1}) d\xi_1 \end{aligned} \tag{3}$$

Let $\mathbf{\Phi} = \{\phi_1, \phi_2, \phi_3, \phi_4\}^T$ be the co-state vector. If $\mathbf{\Phi}$ satisfies the following adjoint equations and boundary conditions, then δI can be expressed as a function of $\mathbf{\Phi}$, the flow variables $\mathbf{w}$, and the geometric variations. It no longer has explicit dependence on variations of the flow variables. The adjoint equations are

$$\mathbf{A}_i^T \frac{\partial \mathbf{\Phi}}{\partial x_i} = 0 \quad \text{in } \mathcal{D} \tag{4}$$

in which the $\mathbf{A}_i$ are the Jacobian matrices of the Euler equations, and $\mathcal{D}$ is the domain.

B. Boundary Conditions

The boundary conditions for the adjoint equations are

$$n_1\phi_2 + n_2\phi_3 = (p - p_d) \quad \text{on } B_W \tag{5}$$

$$\int_{B_C} n_i \mathbf{\Phi}^T \mathbf{A}_i \delta \mathbf{w} dB_C = 0 \tag{6}$$

where, B_C is the outer boundary of the domain, and (n_1, n_2) is the unit normal vector pointing out from the flow field. Then δI can be expressed as the following

$$\begin{aligned} \delta I &= \frac{1}{2}\int_{B_W} (p - p_d)^2 \delta(\frac{dB_W}{d\xi_1}) d\xi_1 \\ &\quad + \int_{\mathcal{D}} \{\frac{\partial \mathbf{\Phi}^T}{\partial \xi_1}[\delta(\frac{\partial y}{\partial \xi_2})\mathbf{f}_1 - \delta(\frac{\partial x}{\partial \xi_2})\mathbf{f}_2] \\ &\quad + \frac{\partial \mathbf{\Phi}^T}{\partial \xi_2}[-\delta(\frac{\partial y}{\partial \xi_1})\mathbf{f}_1 + \delta(\frac{\partial x}{\partial \xi_1})\mathbf{f}_2]\} d\xi_1 d\xi_2 \\ &\quad + \int_{B_W} \phi_2 \delta(-\frac{\partial y}{\partial \xi_1}) + \phi_3 \delta(\frac{\partial x}{\partial \xi_1}) p d\xi_1 \end{aligned} \tag{7}$$

Once $\mathbf{\Phi}$ is solved, Equation (7) can be evaluated without additional flow field evaluations.

Reuther[16] and Wang[17] mentioned that the boundary condition (6) may be simplified by setting $\mathbf{\Phi}$ to zero on the far boundary provided the far boundary is far enough for external flow problems. For internal flows where B_C is close to B_W, the above simplified boundary condition should not be used. Instead, the characteristic wave method is applied here. Time derivative terms are added to the adjoint equations and they become

$$\frac{\partial \mathbf{\Phi}}{\partial t} - \mathbf{A}_i^T \frac{\partial \mathbf{\Phi}}{\partial x_i} = 0 \quad \text{in } \mathcal{D} \tag{8}$$

Thus the adjoint equations can be solved by time-marching methods. They have the same characteristic wave paths as the Euler equations, but, because of the minus sign, the wave propagation directions are opposite to those of the Euler equations. This property is important for assigning boundary values on the outer boundary.

The boundary B_C can be divided into three parts: the two periodic boundaries B_{CP}, the inlet B_{CI}, and the exit B_{CE}. For the periodic boundaries, if $\mathbf{\Phi}$ satisfies the periodic boundary condition, then

$$\int_{B_{CP}} n_i \mathbf{\Phi}^T \mathbf{A}_i \delta \mathbf{w} dB_C = 0 \tag{9}$$

For the inlet and the exit, the integrand of Equation (6) is set to zero.

For the inlet, three flow variables are specified according to the flow boundary conditions. Only one degree of freedom is left for the flow variables. In order to let the integrand equal to zero everywhere at

the inlet , the coefficient in front of this free parameter has to be zero. This provides one constraint on the co-state variables on the inlet boundary. Three degrees of freedom are left for the co-state variables and their values can be extrapolated from the inner field.

For the exit, similar derivation can be done. Three constraints are derived on the co-state variables and one value can be extrapolated from the inner field. According to the wave propagation property mentioned above, the way of assigning boundary values for the adjoint equations is very similar to that of the Euler equations. The major difference is just that the wave propagation directions are reversed.

The resultant form of the adjoint boundary conditions on the inlet and exit boundaries are:

$$C_{11}\phi_1+C_{12}\phi_2+C_{13}\phi_3+C_{14}\phi_4=0 \quad \text{at the inlet} \quad (10)$$

$$D_{i1}\phi_1+D_{i2}\phi_2+D_{i3}\phi_3+D_{i4}\phi_4=0 \quad \text{at the exit} \quad (11)$$

in which i=1, 2, 3, and C_{1j}, D_{ij} are functions of flow variables and geometry parameters. At the inlet, three linear combinations of $\phi_1, \phi_2, \phi_3, \phi_4$ are treated as three variables and their boundary values are extrapolated from the inner field. These three combinations are arbitrary as long as they are linearly independent to one another and linearly independent to the left hand side of Equation (10). At the exit, a similar extrapolation is used.

C. Shape Representation

The Hicks-Henne shape functions[16] are used to adjust the shape of the blade. The formulas for these functions are $b_i(x_1) = sin^4(\pi x_1^{m_i})$, $m_i = ln(0.5)/ln(x_{Mi})$. $i = 1, 2, ..., 32$. Sixteen functions for the upper surface and sixteen for the lower surface, respectively. x_{Mi} are pre-selected values corresponding to the locations of maximum b_i. Figure 2 shows the shapes of these functions.

The way the gradient is obtained is as follows. Small perturbations are added to an initial airfoil shape. The perturbations (for both upper and lower surfaces) are

$$\delta y_\beta(x_1) = (\delta c_\beta) \cdot b_\beta(x_1),$$

(no summation convention on β is applied.)

in which $\beta = 1, 2, ..., 32$. c_β is the weight of the shape function b_β . It acts like a design parameter. Perturb each c_β and calculate the resulting variation of the cost function δI_β from Equation (7). Then the β-th component of the gradient is obtained as

$$g_\beta = \frac{\delta I_\beta}{\delta c_\beta}$$

(no summation convention on β is applied.)

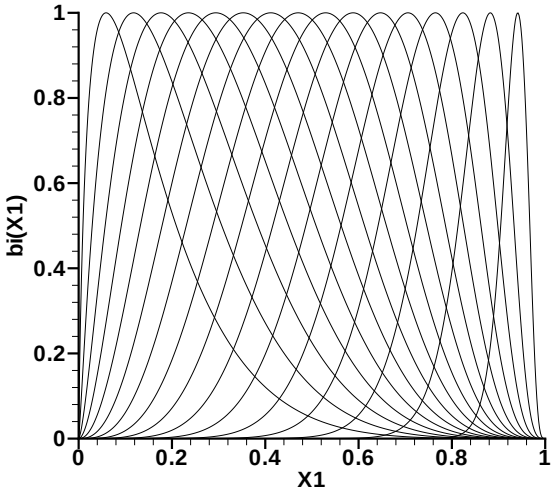

Fig. 2 The Hicks-Henne shape functions.

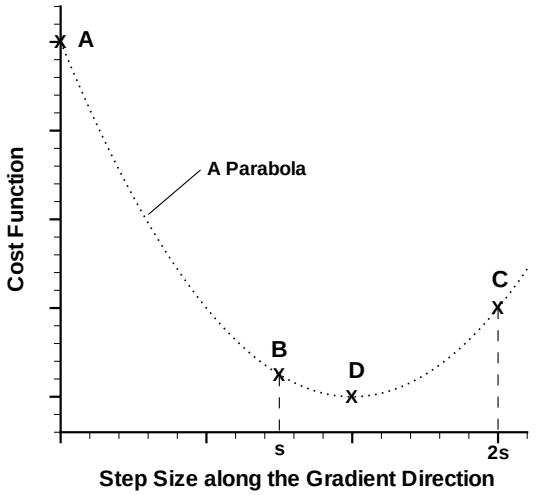

Fig. 3 One-D search method.

Each time the blade shape is perturbed, the mesh needs to be adjusted once. Then Equation (7) can be evaluated. The new mesh can be generated from the mesh generator or by perturbing the old mesh. The latter is faster and hence adopted.

After the gradient is obtained, a 1-D search optimization method is applied to determine the step size along the gradient direction. Figure 3 is a sketch for the 1-D search method. For each design cycle, an initial step size s is given to the program. Denote the initial design by A. Along the gradient direction with a step size s, the program finds a new design, B. Doubling the step size, the program finds another new design, C. If the cost function value of B is smaller than that of A and the cost function value of C is

larger than that of B, then the program uses the three points A, B, and C to perform a parabolic fit and find an approximate local minimum point, D. If the cost function values of A, B, and C do not satisfy the above condition, then the program adjusts the value of s until the condition is satisfied. The step size between A and D is used as the initial step size and D becomes the initial design for the next design cycle. Solutions of the latest design is also used as initial conditions for the next design cycle. At present no constraint is implemented on the design space.

The flow solver and the adjoint equation solver are both modified from a version of Flo52x. Three levels of multigrid are adopted. For this study, the program only deals with steady-state solutions. Time accuracy is not important and therefore local time stepping is adopted. A CFL number of 9 is used.

IV. Results and Discussions

Three design cases are tested for this method: a transonic cascade with the NACA0015 airfoil and the Hobson I and Hobson II supercritical shock-free cascades. The meshes are 160×32 O-grids. They are shown in Figures 4, 5, and 6. For the NACA0015 design case, the solvers converge normally. However, for the Hobson I and the Hobson II design cases, the solvers are sometimes divergent during the design process. Therefore the dissipation on coarser meshes are increased to 1.6 times of its original value to enhance solution convergence. Since the dissipation on the finest mesh remains the same, the precision of the solver is not affected. An example of convergence histories of the Euler solver is shown in Figure 7. The rates of convergence are quite different but the magnitudes of the final maximum residuals are approximately the same. Only single precision (32 bit) operations are used in the current computations.

On the other hand, an example of the convergence histories of the adjoint equation solver is shown in Figure 8. The magnitudes of the final maximum residuals are slightly different for the three design cases. The explanation is that the magnitude of the final maximum residual of the adjoint equation solver is affected by the flow condition. For the NACA0015 design case, if the shock wave locations or strengths are different for the present design and the target design, then the boundary conditions of the adjoint equations are discontinuous at the shock wave locations. This discontinuity possibly causes some difficulties for the adjoint equation solver and therefore the final residual is larger than the other two cases.

During the design process, each flow evaluation uses the result of the previous evaluation as the initial condition. Thus the solver can fully converge faster than it does in the example of Figure 7. This is true for the adjoint solver, too. For the NACA0015 design case, the solvers perform 200 iterations for each evaluation. Each flow evaluation takes approximately 9 seconds, and each adjoint equation evaluation takes approximately 12 seconds on an AMD athlon 1800+ CPU. For the Hobson I and Hobson II design cases, 400 iterations are performed, and the computational time is approximately doubled.

Before the adjoint equation method is applied on any design cases, the gradient calculated by this method is compared with that obtained by direct perturbation and finite-differences to examine its correctness. For the direct perturbation method, the 32 design parameters are perturbed one at a time. For each perturbation of the shape, one flow evaluation

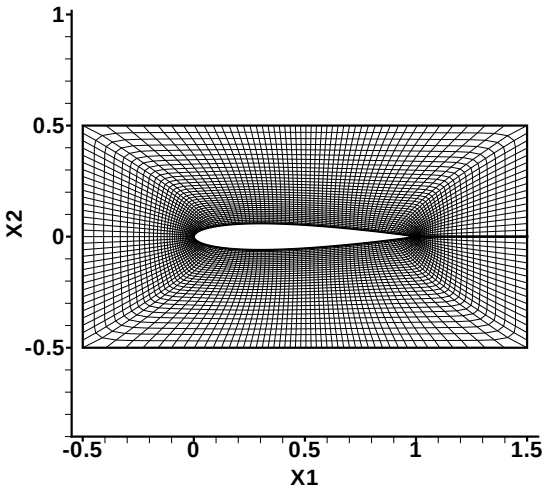

Fig. 4 Mesh for the NACA0015 cascade.

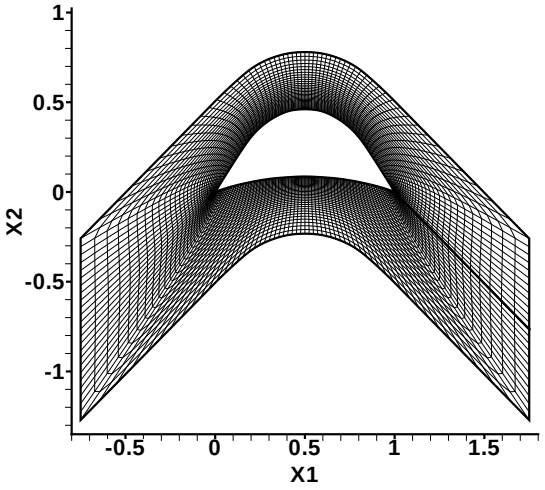

Fig. 5 Mesh for the Hobson I cascade.

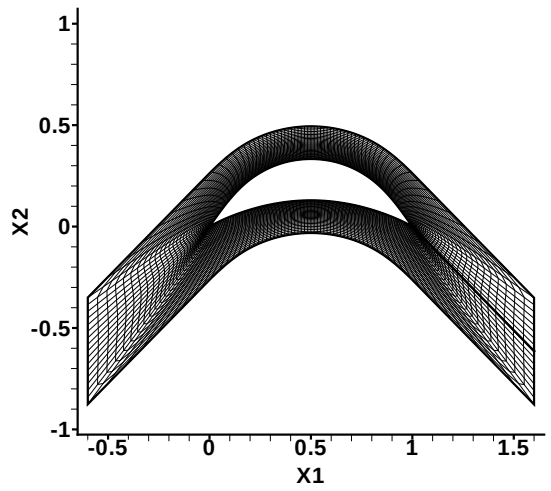

Fig. 6 Mesh for the Hobson II cascade.

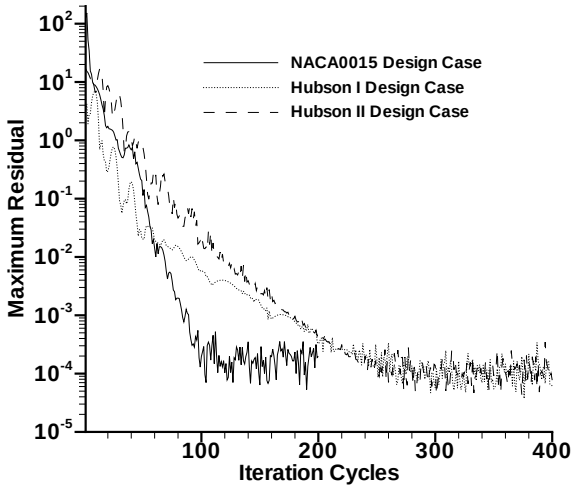

Fig. 7 Convergence history of the Euler solver.

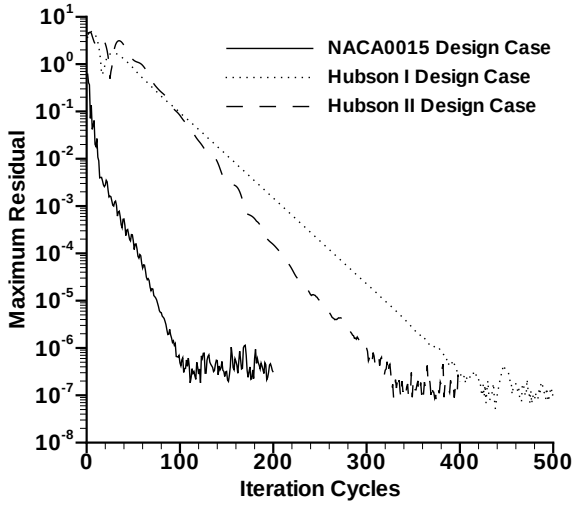

Fig. 8 Convergence history of the adjoint equation solver.

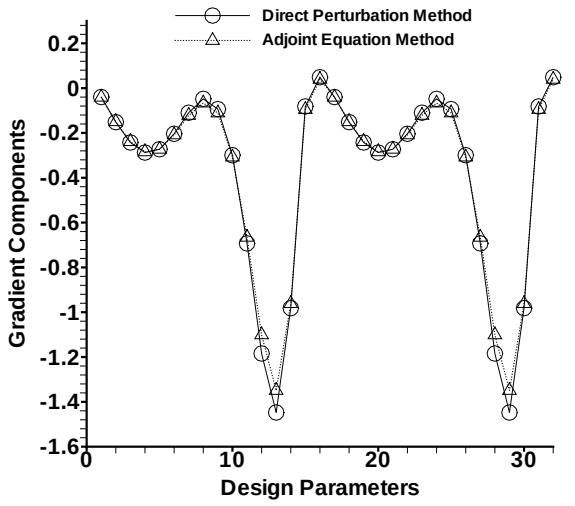

Fig. 9 Comparison of gradients for the NACA0015 cascade case.

is performed in order to evaluate the cost function. Compared to the adjoint equation method, the direct perturbation method takes approximately 32 times of the computational time (excluding one basic evaluation of the flow field that is needed for both methods) to obtain the gradient information. Figure 9 shows the comparison of gradients between the adjoint equation method and the direct perturbation method for the NACA0015 design case for the first design cycle. They match each other well. The locations of largest deviations coincide with the shock wave locations. Details of the three test cases are discussed below.

A. The NACA0015 Cascade

The first case is the cascade of NACA0015 airfoils with zero stagger angle and a unit space to chord ratio. The flow solver is first used to solve the flow through this cascade. Once the solution is obtained, the pressure distribution over the airfoil is calculated and set up as the target pressure. The design code is then applied to obtain the desired airfoil shape starting from the NACA0012 airfoil. The success of the design is then measured by the difference between the final shape obtained by the design code and that of the original NACA0015 airfoil and also the differences of their corresponding pressure distributions. The geometry and the grid used in the computation are shown in Figure 4. The inflow angle is 0 degree with respect to the x_1 axis. A back pressure corresponding to an isentropic exit Mach number of 0.7 is used. The

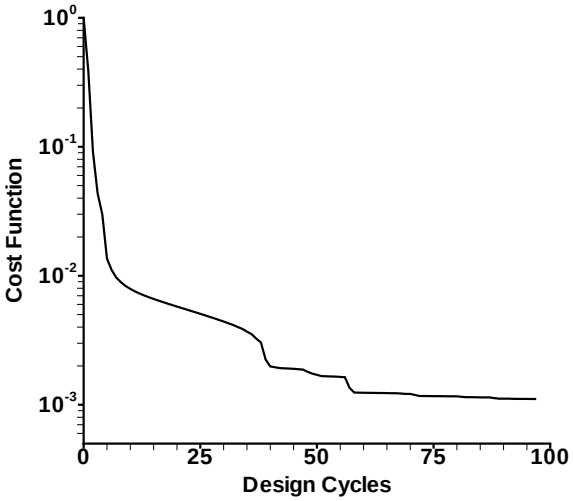

Fig. 10 History of cost function for the NACA0015 cascade case.

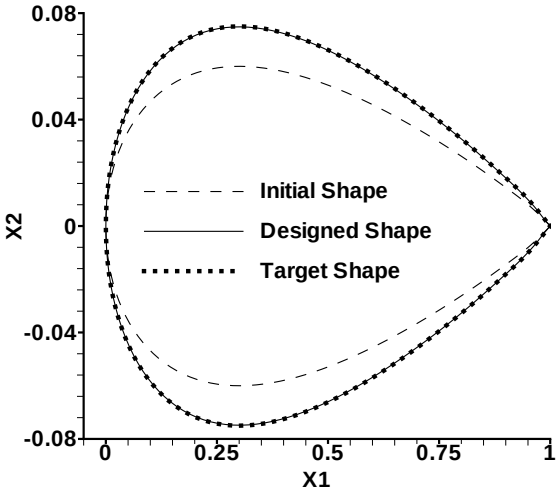

Fig. 11 Comparison of the blade shapes for the NACA0015 cascade case.

Hicks-Henne shape functions, i.e., the location of x_{Mi}, are uniformly distributed along the chord.

Figure 10 shows the history of the cost function. At the 98th design cycle, the program is not able to find a better design within a preset amount of computational effort, and the program stops there. The cost function is reduced by approximately three orders of magnitude. Figure 11 shows the final designed shape as compared to the initial and target shapes. Figure 12 shows the comparison of the corresponding pressure distributions. The designed shape and the pressure distribution match well with the target shape and target pressure distribution, respectively. These results demonstrate the effectiveness of the method for transonic flows with shock waves.

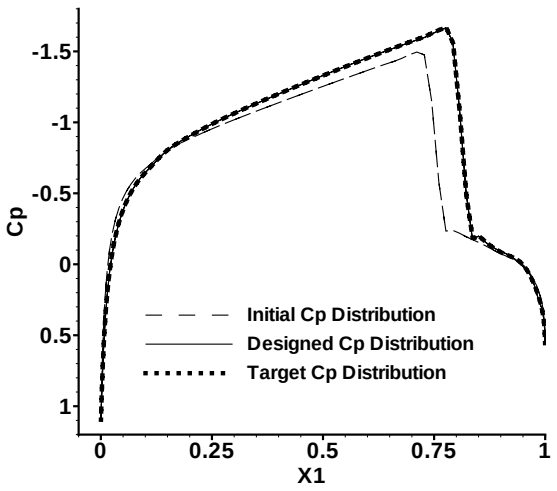

Fig. 12 Comparison of the C_p distributions for the NACA0015 cascade case.

B. The Hobson I Cascade

The second case is the Hobson I shock-free blade. It consists of a thick profile and is designed by the hodograph method to give a shock free supersonic pocket.[3] However, a small perturbation in the flow field can cause the generation of shock waves and hence large changes of the flow. The hodograph design has a space to chord ratio of 1.0121. The inflow angle is 43.544 degrees with respect to the x_1 axis. The design exit Mach number is 0.476. The maximum Mach number in the blade passage is 1.520.

The Mach number distribution from the present Euler flow solver is compared with the hodograph solution in Figure 13. In order to better match the hodograph solution, the exit static pressure is adjusted to 0.997 instead of 1 due to the finite distance of the exit boundary from the blades. Two design approaches are tested, both with the aim of reaching the original Hobson blade shape. The first design approach uses the computed pressure distribution (corresponding to the Mach number shown as dotted line in Figure 13) as the target pressure, while the second approach uses the original hodograph pressure distribution (corresponding to the Mach number shown as solid line in Figure 13) as the target pressure. In both cases, the initial shape is obtained by deforming the original Hobson blade shape. The size in the x_2 direction is shrunk to 0.95 times of its original value. The size in the x_1 direction remains the same. The distribution of the Hicks-Henne shape functions is uniform.

Figure 14 shows the history of the cost function vs. the number of design cycles in the first approach. In

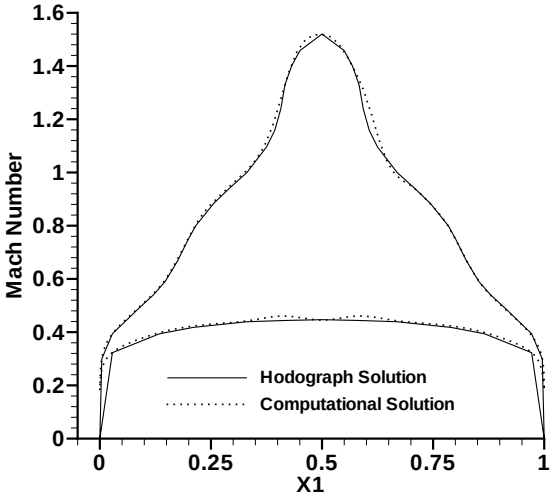

Fig. 13 Comparison between the hodograph solution and the computational solution for Hobson I.

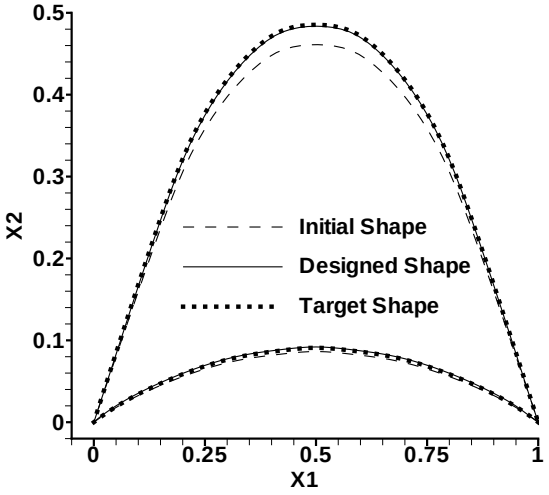

Fig. 15 Comparison of the blade shapes for the Hobson I cascade case with the computational target pressure.

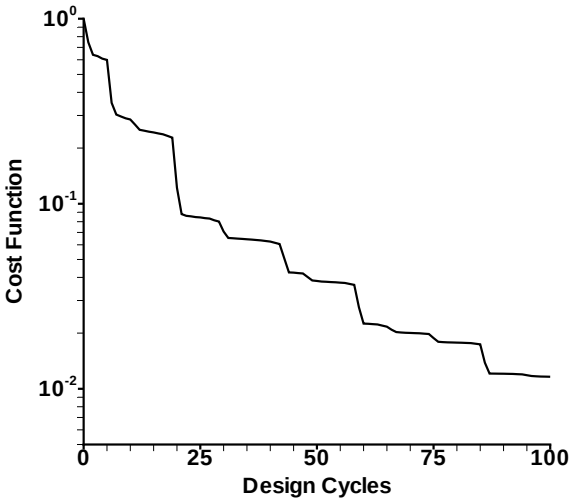

Fig. 14 History of cost function for the Hobson I cascade case with the computational target pressure.

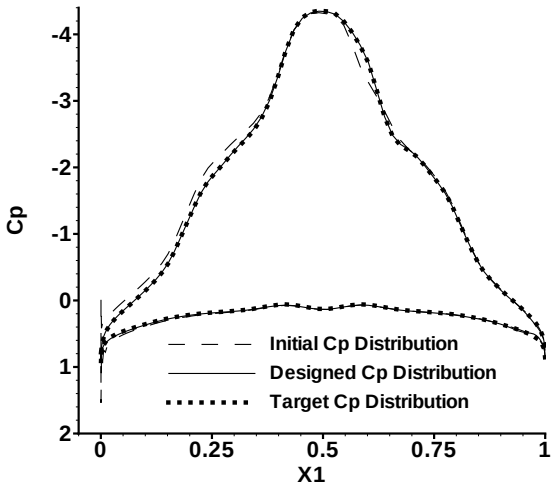

Fig. 16 Comparison of the C_p distributions for the Hobson I cascade case with the computational target pressure.

this case, the cost function does not go down as much as the NACA0015 design case in 100 design cycles. However, the cost function is still decreasing while in the previous case the program reaches its limit at the 98th cycle. The cost function history curve has some flat regions and some sudden drops. This is similar to the behavior in the previous case. Figure 15 shows the final designed shape and compares it with the initial and target shapes. Figure 16 shows their corresponding pressure distributions. The designed shape and pressure distribution are very close to the target shape and pressure distribution, respectively. No obvious shock waves appear. A close examination of Figure 16 shows that the designed pressure distribution has a noticeable deviation from the target pressure distribution near the trailing edge. The reason is that the shape functions are not adequately distributed near the trailing edge, and hence the shape near the trailing edge is insufficiently represented. Although the pressure distribution is not completely determined by the local shape, adding more shape functions near the trailing edge improves the solution (see later discussions). In Figure 16, there is some unphysical fluctuation of the pressure distribution near the leading edge of the

initial shape. For the target shape and the designed shape, there is no such obvious fluctuation.

Figure 17 shows the history of the cost function for the second design approach, where the original hodograph solution is used as the target pressure distribution in the design. Obviously, the cost function ceases to decrease after less than one order of magnitude reduction. In the previous case where the computed pressure distribution of the Hobson I cascade is used as the target pressure, we expect to recover both the original Hobson I blade shape and the target pressure distribution since the same Euler flow solver is used to obtain the flow solutions. This is confirmed by the over two orders of magnitude reduction in the cost function shown in Figure 14 and also the close agreement between the target pressure distribution and that of the designed blade although they differ noticeably from the original hodograph pressure distribution. The hodograph solution is after all a solution from a different numerical method. One cannot expect that the current design method based on a particular numerical method for the Euler equations to fully recover the hodograph design. Consequently, the reduction in the cost function is limited when the hodograph pressure distribution is used as the target function.

Figure 18 shows that the agreement between the designed blade shape and the target shape is not as good as that found in Figure 15. The agreement between the designed pressure distribution and the target hodograph pressure distribution shown in Figure 19 is also not as good as that found in Figure 16. These results are consistent with the above argument. However, the latter design does give the best approximation to the specified hodograph pressure distribution, given the constraint on the number and location of the shape functions (the design space).

C. The Hobson II Cascade

The third case is the Hobson II shock-free cascade.[3] It is thinner than the Hobson I blade. This cascade has a space to chord ratio of 0.5259. The design exit Mach number is 0.575. The maximum Mach number in the blade passage is 1.132. The inflow angle is 46.123 degrees. The Mach number distributions of the hodograph solution and the computational solution are shown in Figure 20. Similar to the Hobson I case, there are visible differences between the computational solution and the hodograph solution. In this case, only the computational target pressure is adopted. The initial shape is a deformed Hobson II blade. The size in the x_2 direction is shrunk to 0.95 times of its original value. The size in the x_1 direction remains the same. The distribution of the Hicks-Henne shape functions is uniform. Figure 21 shows the cost function history. Figure 22 shows the comparison of

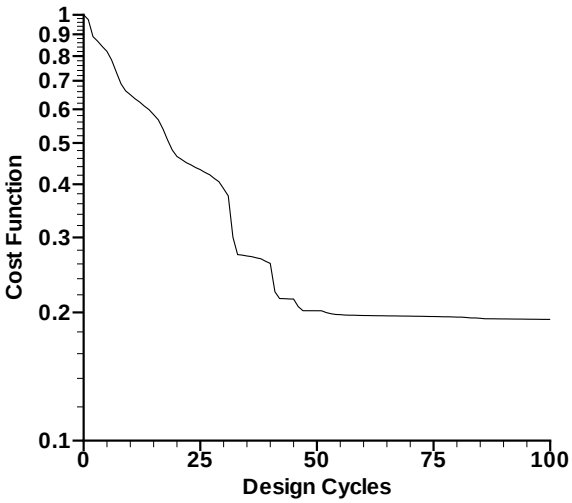

Fig. 17 History of cost function for the Hobson I cascade case with the hodograph target pressure.

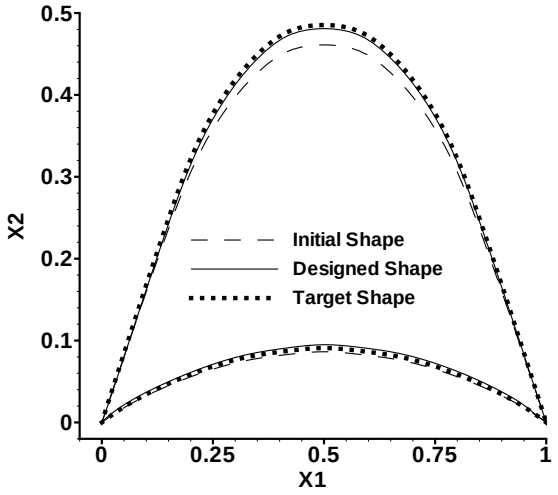

Fig. 18 Comparison of the blade shapes for the Hobson I cascade case with the hodograph target pressure.

the blade shapes. Figure 23 shows the comparison of pressure distributions. The cost function does not go down as much as it does in the Hobson I case with the same type of the target pressure. Nevertheless, the designed shape and pressure distribution are still very close to the target shape and pressure distribution. For the pressure distributions, the deviation from the target pressure near the trailing edge is more obvious in this case. The unphysical fluctuation of pressure at the leading edge of the initial shape is also present.

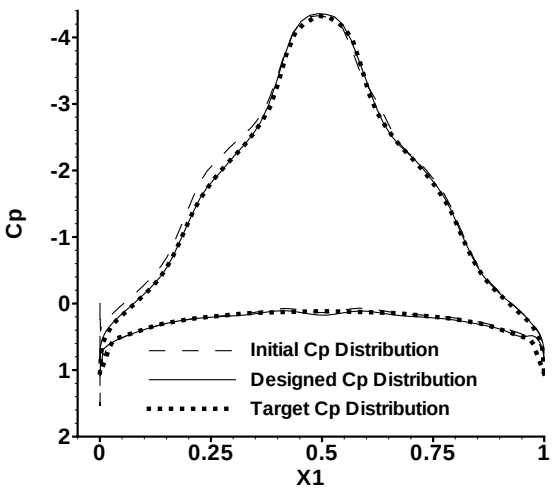

Fig. 19 Comparison of the C_p distributions for the Hobson I cascade case with the hodograph target pressure.

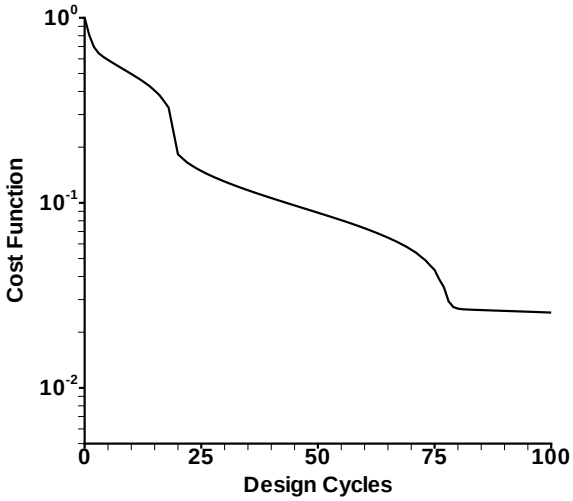

Fig. 21 History of cost function for the Hobson II cascade case.

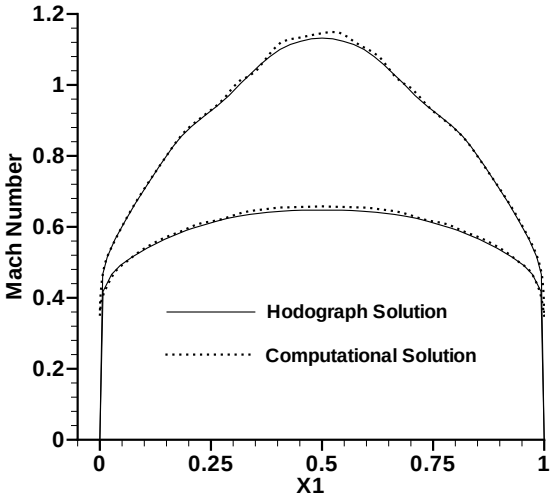

Fig. 20 Comparison between the hodograph solution and the computational solution for Hobson II.

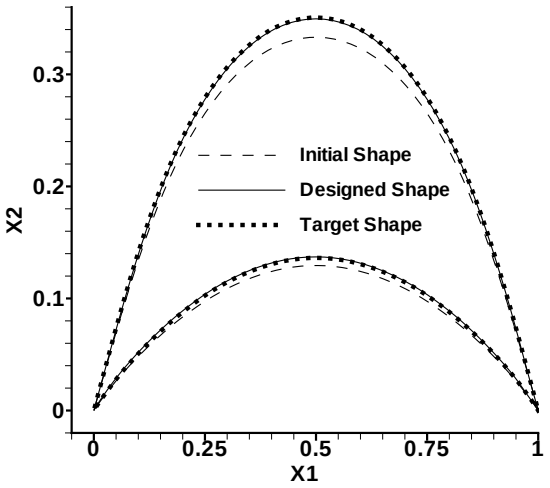

Fig. 22 Comparison of the blade shapes for the Hobson II cascade case.

D. Effect of Shape Functions

The above test cases demonstrate the capability of present design method under different flow conditions and different geometries. The performance of the optimization program depends on the path it can take in the design space. For a given design target, how well one can achieve the target pressure depends on the completeness of the design space. Proper distribution of the shape functions and the number of the shape functions are important parameters. We explore their effect on the performance of our design program for the NACA0015 case.

First the distribution of the shape functions is adjusted. The number of the shape functions remains the same. It is 32. The locations of x_{Mi} for $i = 1, 2, ..., 16$ are chosen to be $0.5 \times [1 - cos(\theta_i)]$. $\theta_i = \pi \times i/17$. For $i = 17, 18, ..., 32$, x_{Mi}=x_{Mj}, and $j = i-16$. The distribution is denser near the leading edge and the trailing edge. The cost function history is shown in Figure 24. At the 59th design cycle, the program reaches its limit and stops.

Secondly, the number of the shape functions are doubled, but the distribution of x_{Mi} remains uniform. The cost function history is also shown in Figure 24. At the 67th design cycle, the program reaches its limit and stops. The original cost function history shown in

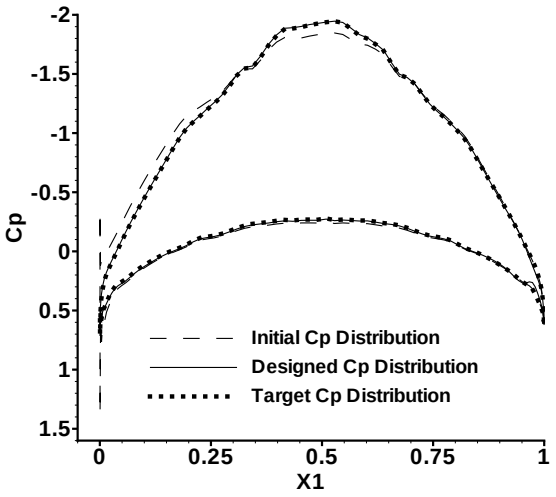

Fig. 23 Comparison of the C_p distributions for the Hobson II cascade case.

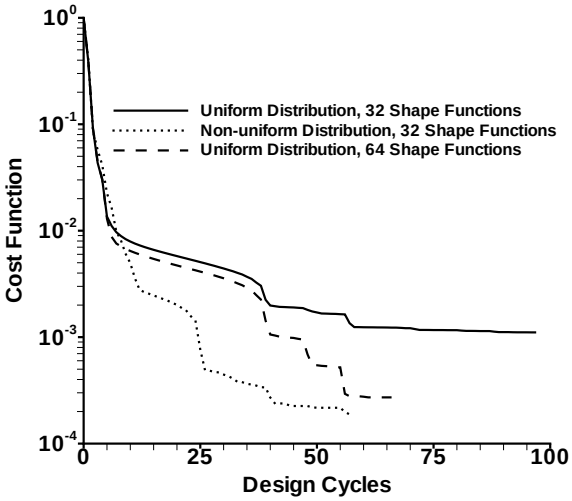

Fig. 24 Performances for different arrangements of design parameters.

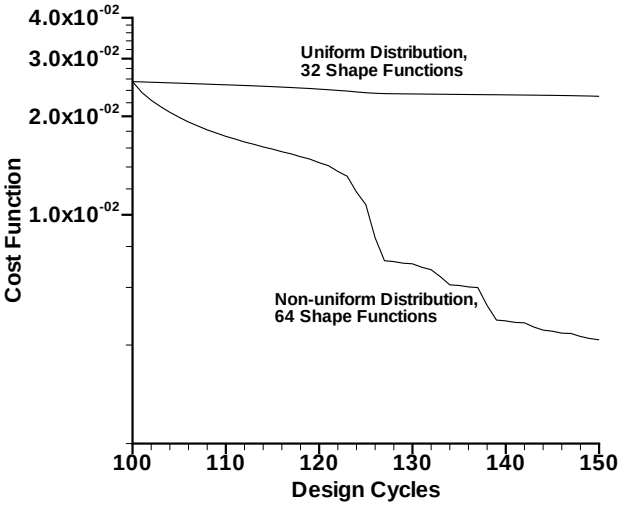

Fig. 25 Effect of changing the distribution of shape functions after 100 design cycles.

Figure 10 is also plotted in Figure 24 as a reference. The computational time needed for solving the adjoint equation is independent of the number of design parameters. However, in order to obtain the gradient information, extra time is needed to perturb the mesh. The time needed for perturbing the mesh is proportional to the number of design parameters. Therefore the number of design parameters needs to be kept in a reasonable range although increasing the number of parameters can improve the precision of the solution. In this study, the number of parameters is 32 or 64. As shown in Figure 24, the computation with non-uniform distribution shape functions gives the best result. It yields the fastest reduction and also the lowest value of the cost function. The second best one is the computation with double the number of shape functions. In this case, choosing better locations to put the shape functions has more benefit than doubling the number of shape functions.

For the Hobson I and Hobson II design cases, if the shape functions are located too close to the leading edge or trailing edge, problems may occur at the initial stage of the design process. For example, sometimes a negative-thickness leading edge or trailing edge may appear during the design process. That causes problems for the flow and adjoint solvers. After 100 design cycles with uniformly distributed shape functions, the design is very close to the target. The step size of shape modification is smaller than that at the beginning of the design process. At this stage, the problem mentioned above is less likely to occur so that we may shift to use non-uniformly distributed shape functions in order to obtain a better design. For the Hobson II design case, the number of shape functions is increased to 64 and distributed nonuniformly after the first 100 design cycles to see if it can give a better result. The computation is continued for another 50 design cycles. The history of the cost function for the additional design cycles is shown in Figure 25. The corresponding pressure distributions near the trailing edge are shown in Figure 26. The solution near the trailing-edge of the blade is significantly improved when the number of shape functions is increased and the non-uniform distribution is adopted. During the design cycles, the distribution of shape functions can be modified if different distributions are needed for different design stages. More study is needed to determine the

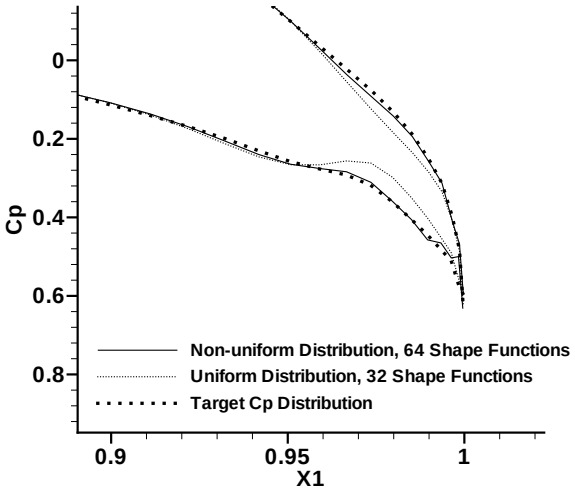

Fig. 26 C_p distributions near the trailing edge after 150 design cycles.

optimum number and distribution of the shape functions for a given design case.

V. Conclusions

An adjoint equation method based on the Euler equations is developed for the aerodynamic design of cascade blades. Three test cases involving a transonic cascade using the NACA0015 airfoil and the Hobson I and Hobson II supercritical but shock-free cascades are studied. The adjoint formulation and boundary conditions are derived by using cost functions based on the square integral of the deviation from a specified target pressure distribution over the blade surface. Gradient information can be obtained with little dependence on the number of design parameters. A 1-D search algorithm is used to accelerate convergence to the design point. Results for the three test cases demonstrate that this method is effective and efficient for the design of transonic and supercritical turbomachinery cascade blades. The choice of the number and locations of shape functions, however, may significantly influence the efficiency and accuracy of the design. Better performance can be obtained by dynamically adjusting the number and distribution of the shape functions during the design process.

References

[1]Lighthill, M., "A New Method of Two Dimensional Aerodynamic Design," ARC R. & M. 2112, 1945.

[2]Bauer, F., Garabedian, P., and Korn, D., *Supercritical Wing Sections, Lecture Notes in Economics and Mathematical Systems, vol. 66*, Springer-Verlag, New York, 1972.

[3]Hobson, D. E., "Shock-Free Transonic Flow in Turbomachinery Cascades," Department of engineering report cued/a turbo/tr 65, University of Cambridge, 1974.

[4]Tan, C. S., Hawthorne, W. R., McCune, J. E., and Wang, C., "Theory of Blade Design for Large Deflections: Part II - Annular Cascades," *Journal of Engineering for Gas Turbines and Power*, Vol. 106, 1984, pp. 354–365.

[5]Giles, M., Drela, M., and Thompkins, W. T., "Newton Solution of Direct and Inverse Transonic Euler Equations," AIAA Paper 85–1530, AIAA 7th Computational Fluid Dynamics Conference, Cincinnati, Ohio, June 1985.

[6]Dang, T. and Isgro, V., "Euler-based inverse method for turbomachine blades: Part I – two-dimensional cascades," *AIAA Journal*, Vol. 33, No. 12, Dec. 1995.

[7]Dang, T., Damle, S., and Qiu, X., "Euler-based inverse method for turbomachine blades: Part II – three dimensions," *AIAA Journal*, Vol. 38, No. 11, Nov. 2000.

[8]Hicks, R. M., Murman, E. M., and Vanderplaates, G. N., "An Assessment of Airfoil Design by Numerical Optimization," NASA TM X-3092, NASA Ames Research Center, Moffett Field, California, July 1974.

[9]Reuther, J., Cliff, S., Hicks, R., and Van Dam, C., "Practical Design Optimization of Wing/Body Configurations Using the Euler Equations," AIAA Paper 92–2663, 1992.

[10]Hager, J., Eyi, S., and Lee, K., "Design Efficeincy Evaluation for Transonic Airfoil Optimization: A Case for Navier-Stokes Design," AIAA Paper 93–3112, AIAA 24th AIAA 24th Fluid Dynamics Conference, Orlando, Florida, July 1993.

[11]Jameson, A., "Aerodynamic Design via Control Theory," *Journal of Scientific Computing*, Vol. 3, 1988, pp. 233–260.

[12]Jameson, A., "Optimum Aerodynamic Design Using CFD and Control Theory," AIAA Paper 95–1729, AIAA 12th Computational Fluid Dynamics Conference, San Diego, California, june 1995.

[13]Reuther, J. and Jameson., A., "Aerodynamic Shape Optimization of Wing and Wing-Body Configurations Using Control Theory," AIAA Paper 95–0123, AIAA 33rd Aerospace Sciences Meeting, Reno, Nevada, January 1995.

[14]Reuther, J., Alonso, J. J., Rimlinger, M. J., and Jameson, A., "Aerodynamic Shape Optimization of Supersonic Aircraft Configurations via an Adjoint Formulation on Distributed Memory Parallel Computers," *Computers and Fluids*, Vol. 28, No. 4-5, 1999, pp. 675–700.

[15]Jameson., A. and Vassberg, J. C., "Computational Fluid Dynamics for Aerodynamic Design: its current and future impact," AIAA Paper 2001–0538, AIAA 39th Aerospace Sciences Meeting, Reno, Nevada, January 2001.

[16]Reuther, J., "Aerodynamic Shape Optimization Using Control Theory," NASA Technical Report NASA-CR-201064, NASA Ames Research Center, 1996.

[17]Wang, L., "Transonic Airfoil Optimum Design Based on Control Theory," Thesis, Northwestern Polytechnical University, Xi'an, China, 1999.